Nanoscale

Mesoscopically Structured Nanocrystalline Metal Oxide Thin Films

Journal:	*Nanoscale*
Manuscript ID:	NR-REV-05-2014-002909.R1
Article Type:	Review Article
Date Submitted by the Author:	13-Jul-2014
Complete List of Authors:	Carretero-Genevrier, Adrian; Laboratoire de Chimie de la Matière Condensée de Paris, Collège de France Drisko, Glenna; Université Pierre et Marie Curie Paris 6, CNRS, Laboratoire de Chimie de la Matière Condensée de Paris, Boissière, Cédric; Laboratoire de Chimie de la Matière Condensée de Paris, Collège de France Grosso, David; Laboratoire de Chimie de la Matière Condensée de Paris, Collège de France Sanchez, Clement; Universite Pierre et Marie Curie,

Mesoscopically Structured Nanocrystalline Metal Oxide Thin Films

By Adrian Carretero-Genevrier,[a,b,†] Glenna L. Drisko,[b,c,†] David Grosso,[b,d] Cédric Boissiere[b,e] and Clement Sanchez[b,d,e,*]

[a] Institut des Nanotechnologies de Lyon (INL) CNRS- Ecole Centrale de Lyon, 36 avenue Guy de Collongue, 69134 Ecully, France

[b] Collège de France, UMR 7574, Chimie de la Matière Condensée de Paris, F-75005, Paris, France. Fax: +33-144271504; Tel: +33-144271501; E-mail: clement.sanchez@college-de-france.fr

[c] Laboratoire de Chimie de Coordination, CNRS UPR8241, 205, route de Narbonne, 31077 Toulouse, France.

[d] Sorbonne Universités UPMC Univ Paris 06, UMR 7574, Chimie de la Matière Condensée de Paris, F-75005, Paris, France.

[e] CNRS, UMR 7574, Chimie de la Matière Condensée de Paris, F-75005, Paris, France.

Fax: +33-144271504; Tel: +33-144271501;

† These authors contributed equally to this work

Abstract

This review describes the main successful strategies that are used to grow mesostructured nanocrystalline metal oxide and SiO_2 films via deposition of sol-gel derived solutions. In addition to the typical physicochemical forces to be considered during crystallization, mesoporous thin films are also affected by the substrate-film relationship and the

mesostructure. The substrate can influence the crystallization temperature and the obtained crystallographic orientation due to the interfacial energies and the lattice mismatch. Mesostructure can influence crystallite orientation, and affects nucleation and growth behavior due to the wall thickness and pore curvature. Three main methods are presented and discussed: templated mesoporosity followed by thermally induced crystallization, mesostructuration of already crystallized metal oxide nanobuilding units and substrate-directed crystallization with an emphasis on very recent results concerning epitaxially grown piezoelectric structured α-quartz films via crystallization of amorphous structured SiO_2 thin films.

I. Introduction

The synergetic coupling between inorganic or hybrid sol-gel chemistry, soft matter physics, and smart processing has opened new avenues for advanced materials research.[1] In the past ten years, an increasing quantity of mesostructured materials with very diverse chemical compositions (oxides,[2] metals,[3] carbons,[4] chalcogenides,[5] semi- conductors,[6] etc.) deposited as thin films have appeared, and the reader is referred to some excellent reviews of such materials.[7-17] The crystallization of inorganic structured materials presents a variety of challenges. Here we will be discussing the preparation of and theory behind mesostructured crystalline metal oxide and SiO_2 thin films. Additionally, this short review describes some relevant research directions that still must be developed in more depth to produce new insights in this young field.

Among mesostructured materials, metal oxides are inexpensive, stable, mostly nontoxic and present a large set of interesting optical, electronic, and magnetic properties that open access to promising applications as low-k materials, membranes and separation devices, functional smart coatings, fuel and solar cells, microbatteries, catalysts, sensors, and

others.[12,18-20] The physical responses and thus properties of many metal oxides are strongly dependent on their size, shape, morphology, crystallinity, and exposed crystallographic faces.[21-23] Examples of physical properties arising from crystallization include: magnetism,[24] piezoelectricity,[25-26] sorption behavior,[27] photocatalytic activity,[28-29] and increased material stability over the amorphous counterpart.[30] Therefore the controlled design of mesoscopically architectured nanocrystalline metal oxide thin films is of paramount importance.

Three main strategies depicted in Figure 1 can be used to structure crystalline films via solution deposition techniques: i) electroless chemical etching of a crystalline substrate,[31] ii) assembly of crystalline nanobuilding blocks (NBBs) via evaporation induced self-assembly (EISA),[32-34] and iii) crystallization of pre-assembled structures[35] (Figure 1). We will not cover non-solution routes to form mesoporous crystalline films in this review.[36] Typical transmission electron microscope images (TEM) representing the state of the art in mesoscopically architectured nanocrystalline metal oxide films are also displayed in Figure 1. These three methods all present advantages and limitations.

Figure 1. Three chemical solution methods to create mesoporous materials. (a) Chemical etching is performed to drill into a metallic film, which is then oxidized to form a mesoporous metal oxide. The SEM (left) and TEM (right) images are from a silicon substrate patterned with Ag, and then etched in dilute hydrofluoric acid to produce mesoporous nanowires. Microscopy images reproduced with permission from reference 37. (b) Nanobuilding blocks are aggregated around micelles through EISA before organic matter is removed, often through thermal decomposition. The SEM (left) and TEM (right) images are of a Nb doped anatase TiO_2 film prepared from pre-crystallized particles assembled with Pluronic F127. Microscopy images reproduced with permission from reference 38. (c) Deposition of hydrolyzed molecular precursors, originating from molecules such as $Si(OEt)_4$ and $TiCl_4$, along with a

self-assembling surfactant can lead to ordered mesoporosity. In the TEM images $ZnTiO_3$ templated with Pluronic F127 is viewed from the [110] and [001] directions. Microscopy images reproduced with permission from reference 39.

Metal assisted chemical etching requires two steps. First metallic domains or nanoparticles are deposited onto a crystalline substrate via physical or chemical processing. Then the patterned substrate is submerged in an etching solution. The crystalline substrate is stable in the etchant, but the substrate in contact with the metal is oxidized and then dissolved (Figure 1a). Non-electrolytic chemical etching can be easily performed, and various 2D shapes can be created related to the morphology and arrangement of the deposited metal nanoparticles. The doping and crystallographic orientation of the substrate are pre-optimized. But, as this technique depends on preferential etching along a particular crystallographic direction, morphology can be controllably tailored only in 2 directions and currently is limited to Si, SiGe, SiC, Ge, GaAs and GaN substrates. The remaining material can (and often naturally does) convert to the corresponding oxide after etching is completed. This topic has been thoroughly discussed in a recent review.[40]

The assembly of crystalline NBBs consists of synthesizing and crystallizing nanoparticles and then depositing them along with a structure directing agent on a substrate (Figure 1b). This approach allows one to tune the size, chemical composition, crystallinity and particle shape of the inorganic components, as long as the post-thermal treatment step is mild enough to avoid extensive sintering and loss of porosity. When NBBs are coupled with amphiphilic templates, their size should be tailored to the size of the hydrophilic component of the template.[33] A critical nanoparticle size in relationship to the micelle diameter must not be exceeded to avoid production of inhomogeneous structures.[41]

The post-crystallization method is the most common approach to mesostructured crystalline

thin films via solution deposition. Typically this route entails the EISA of metal oxide precursors around amphiphilic organic constructs, followed by thermally induced crystallization and template removal (Figure 1c). The mesostructure is highly dependent on the solution chemistry (porogen/precursor ratio, acidity) and processing conditions (humidity, temperature, aging, etc.).[42-43] The chemistry of surfactants and block copolymers plays a major role in the stability of the mesostructure during crystallization. Amorphous mesoporous materials of an impressive variety of architectures, mesopore sizes, and chemical compositions can be obtained.[44] Crystallization of these preassembled nanostructures often leads to loss of porosity, inhomogeneous nucleation and crystal growth, and reorganization of the mesostructure during thermal or pressurized treatment. This architectural destruction is due to the fact that in many oxides the activation energy of crystallization is higher than that of structural reorganization.[45]

The strategies described in the present review are all based on thin film deposition of sol-gel derived solutions. Most of the successful routes imply the sol-gel chemistry of highly charged inorganic ions that lead to amorphous-locally ordered NBBs, in the absence of anionic competitors that can form non-oxide basic salts, typical of M(II) oxides. Because of the presence of a substrate, a template or the inherent heterogeneities of colloidal solutions, the nucleation step of crystallization can be generally considered as heterogeneous. To shed light on some selected advances in the field, and for the sake of clarity, this review is split into three main subtopics: i. The templated mesostructuration followed by a crystallization step, ii. The mesostructuration of already crystallized particles and iii. Substrate-directed crystallization, with an emphasis on very recent results that concern epitaxially grown piezoelectric quartz films.[25-26] The fundamental aspects and synthetic techniques will be presented without going into an exhaustive list of materials due to the fact that not all oxides are easily processed into mesoscopically architectured crystalline thin films using solution

based chemistry. Other physical deposition/ablation methods to synthesize nanostructured oxide films will not be discussed as this has been well reviewed elsewhere.[46-47]

II. Background

Ordered pore arrays with controllable pitch and pore size can be obtained by surfactant templating through EISA.[48] EISA consists of depositing a solution containing metal oxide precursors and porogens (*e.g.* amphiphilic block copolymers, surfactants) dispersed in a volatile solvent which self-assemble into periodic structures during solvent evaporation. Often water is present in the initial solution to hydrolyze the metal oxide precursors, and acid is typically either added or generated by hydrolysis, slowing the precursor condensation rate. Other ligands may be added to inhibit premature condensation, particularly acetyl acetone.[49-50] Once a stable solution of miscible species is obtained and aged for the appropriate amount of time, the solution is deposited as a thin film typically using either spin,[51] spray,[52] or dip coating (Figure 2).[53-54] Evaporation begins to evolve the structure within seconds of film deposition.[42,55] Dip coating tends to generate the most homogeneous films over a large surface compared to the other techniques for materials cast from sol-gel solutions, and hence it is the most frequently used method. A successful deposition depends upon a good degree of wetting. If the solution dewets from the substrate surface, islands of inhomogeneous material will be deposited. Dewetting results from high surface tension and can be circumvented by changing the quantity of water (typically increasing alcohol content) or by changing the hydrophobicity (via fluorination, organic modification of the surface or deposition of an inorganic barrier layer) or hydrophilicity (by using heat or acid to oxidize the surface). EISA has been used to prepare mesoporous crystalline thin films of a large variety of oxides (Table 1).

Figure 2. Preparation followed by thermally induced crystallization of mesoporous thin films from deposition of a film of block copolymers (BCP) and inorganic precursors/nanobuilding blocks (I). Here a deposition of two layers of micelles is depicted, though anywhere between a monolayer and over a dozen layers can be deposited in a single coating.

Table 1. Crystalline mesostructured materials.

Crystal polymorph	Crystallite size (nm)	Pore diameter (nm)	Mesostructure	Physical properties	Reference
γ-Alumina	5	13-24	*Fm3m* Face-centered cubic		56
	<5	~8.5	cage type *Im3m*		57
		35-80	hexagonal		58
β-Bi_2O_3	11-14	14-16	Cubic	Photocatalytic activity	59
CeO_2	3-7	3-16.5	Cubic, hexagonal		60
CeO_2 (cerianite)	7.6	9-10	Cubic		61
CeO_2 (cubic)	2-13	14	Cubic	Pseudocapacitive charge storage	62
NiO/Ga doped CeO_2	12				63
Er_2O_3 (cubic)	3-13	15-17	Cubic		64
	16-25	9-13	Grid-like	Luminescence	65
α-Fe_2O_3	13-14	14-15	Disordered		66
	2-7	48-140	Disordered	Photoelectrochemistry	67
	7-10	10	Cubic	Electrochemical properties	68
HfO_2 (monoclinic)	10	14-16	Cubic		69
IrO_2	16	4-11	Grid-like	Electrocatalytic activity	70
$Li_4Ti_5O_{12}$ (cubic)	11-15	18	Cubic	Charge storage, electrical conductivity	71
Periclase MgO (cubic)	5-7	18	Local order		72
α-MoO_3	40-45	13	Cubic	Electrochemical properties	73
Nb_2O_5	<1.0	5.0	Hexagonal		74-75
T-Nb_2O_5 (orthorhombic)	21-46	13-15	Hexagonal	Pseudocapacitive charge storage	76

Rutile RuO_2	3.8	10.2-13.5	Disordered	Electrochemical properties	77
α-quartz SiO_2	40	40	2-D hexagonal	Piezoelectricity	25-26
Cassiterite SnO_2	3.0	6.8	Hexagonal		75
	2.8-7.4	7.8	Hexagonal	Semiconductor E_g=4:05 eV	78
	2	14	*Im3m*		74
	5-6	6.7-14.2	*Im3m*		79
	7-15	1.6-9		CO sensing	80
	2-6	6.7-14.2	Distorted cubic		79
Sb, Nb, Ta Rutile SnO_2 (tetragonal)	2-8	13-14	Cubic	Transparent conducting oxides	81
perovskite $SrTiO_3$	10-20	12	Distorted cubic		82
Ta_2O_5	<1.0	5.0	Hexagonal		75
	<1.0	3.5	Hexagonal		74
L-Ta_2O_5	42	13-15	Hexagonal		76
RuO_2	25-120	30	Hexagonal	Electrodes	83
Anatase TiO_2	8	5-12	Cubic		84-85
	3.0	6.5	Cubic		74
	11.2	16	Cubic	Photoanode	86
	10	10	Cubic (*Im3m*)		87
	5.5		Cubic	Photocatalytic activity	88
	3-8	~10	Cubic, hexagonal, lamellar		89
	>10	5.8	*Im3m*		90
	7-8.5		*Im3m*	Photocatalytic activity	91
	11-17	6.4-11.7	*Im3m*, grid-like	Photocatalytic activity	92
	7-8	2.9-7.6	Grid-like	Electroactivity	93
	2.4	6.5	Hexagonal		75
		7	2D hexagonal (*p6m*)		94
	5-10	3.06-4.88	2D hexagonal (*p6m*)		95
	7.8-10.3	7.6	2D hexagonal (*p6m*)		96
	9-15	5	3D-hexagonal (*R-3m*)		97
	2-13	~5	3D-hexagonal		98
	20-29	7.6-21.1	3D-hexagonal (*R-3m*)		32
	12, 19	21, 18	Gyroid	Photoanode	99
	>2, loss of mesostructure	2.0	*p6m* and wormlike		100
Rutile TiO_2	14-16	5	Ill-defined		101
Eu doped Anatase TiO_2	7-12	5.8-9.5	Grid-like	Charge carrier trapping	102
Nb doped TiO_2	4-14	10	Wormhole and cubic	Electrical conductivity	38

Nb_2O_5 doped TiO_2	12	7	Cubic *Im3m*	Photovoltaics	103
Anatase and Ilmentite TiO_2-$NiTiO_3$	8-20	5	*Im3m* and grid-like		104
V_2O_5	52	12		Photocatalytic H_2 production	105
WO_3		4-8	Disordered	Electrochromic properties	106
	2.0	5.0	Hexagonal		74-75
WO_3 (monoclinic)	17-30	7.3-12.5		Photoelectrochemical activity	107
	12-13	14	Cubic	Electrochromic activity	66
	13	12-13	Cubic	electrochemical/electro chromic	108
WO_3 (cubic)		3.8	Cubic (*Ia3d*)	Hydrogen electrochemical reduction	109
WO_3 (hexagonal, tetragonal, orthorhombic)	20-90	15-30	Wormhole	Color bleaching	110
Y_2O_3-ZrO_2 (monoclinic and tetragonal)	3-4	3.6	2D-hexagonal (*p6mm*)		111
europium doped Y_2O_3	10-17	8.5-14	Disordered	Luminescence	112
$ZnTiO_3$ (cubic)	3-4	3-4.5	Hexagonal	Photoluminescence	39
ZrO_2 (monoclinic)	10	9-10	Distorted cubic		61
ZrO_2 (tetragonal)	2.0	6.2	Cubic		74-75
	3-4	4-5	Hexagonal		111
		15.5	2D-hexagonal		113
	1.5	5.8		Dielectric	74-75
	4-10	2.5			90
Eu and Ag doped ZrO_2 (tetragonal)	6	5-10		Luminescence	114

Several strategies exist to prevent structural collapse during the crystallization of mesoporous thin films. The crystallite to pore size ratio is very important: if the crystallite size becomes larger than the pore size, the mesostructure is usually lost. Crystal growth is limited by feed stock, thus if pore:wall diameter ratio is correct, the morphology can be maintained. In some cases, additives can be used to increase the homogeneity of nucleation.[25-

[26] Crystallization treatment (temperature, duration, pressure) can be varied to optimize the crystals nucleation and the average final crystal size. Using non-combustible templates coupled with a reducing gas during heat treatment, can also retard crystal growth by limiting diffusive sintering.[115] For example, some surfactants carbonize, thus providing mechanical support during the crystallization process. An alternative option is to use optimized heat treatment conditions. For example, prolonged heat treatment at the maximum temperature before the onset of crystallization stabilizes the amorphous network by increasing the activation energy of structural rearrangement.[50,79,84,90] Rapid thermal annealing at high temperature can well preserve the structure by taking advantage of the higher kinetic rate of crystallization over structural rearrangement.[85,116] Another strategy consists of mixing two oxides to inhibit crystallite growth and then to control their size[38,117] or stabilizing a crystallizable oxide (e. g. TiO_2) with an amorphous oxide (e. g. SiO_2).[118] A final consideration is the hydrophobicity of the micellar core, as weakly hydrophobic cores can solvate inorganic nanobuilding blocks, leading to crystal nucleation within the micelle and subsequent structural collapse.[119]

To obtain a homogeneous and well-ordered mesoporous thin film from an ethanolic/aqueous solution, its best to use a substrate with a high surface energy, such as Si with a native oxide layer (0.14 J m^{-2}) or TiO_2 (0.280–0.380 J m^{-2}) rather than glass (0.06-0.08 J m^{-2}) or ITO coated glass (0.05 J m^{-2}).[120]

Cracks are sometimes formed when films need to relieve mechanical stress induced by the contraction of the sol-gel network during condensation (that is during its drying and/or thermal treatments). The mechanical stress of a supported film increases with its thickness. If the ratio (cohesive strength)/(adhesion strength) is high, the layer delaminates. If it is low, the layer cracks due to inhomogeneities in capillary forces. A slow and progressive thermal treatment and/or slowing evaporation rate (*e.g.* using a solvent of higher boiling point,

increasing the humidity and/or lowering the temperature in the dip-coating chamber) can give the film time to reorganize without cracking.[120] For example, the use of 1-butanol in place of ethanol avoided cracking.[96] Cracks can also be avoided by adding nanoparticle filler such as Degussa P25, which decreass the global contraction of the mesostructure, thus decreases the stresses.[121-123]

Film characterization depends principally upon grazing incidence small angle X-ray scattering (GI-SAXS) and ellipsometry. GI-SAXS is used to determine d-spacing and pore symmetry from the analysis of the diffraction patterns. Ellipsometry gives information about the refractive index, thus the film thickness and crystallinity, but also can be used in conjunction with solvent sorption to give information about pore size distribution.[124] Atomic force microscopy (AFM), and scanning electron morphology (SEM) give information about the topology, where grated films can be imaged with transmission electron microscopy (TEM). To assess crystallinity, selected area electron diffraction (SAED) patterns and wide angle X-ray diffraction (WAXS) are typically used.

III. Nanostructuration followed by crystallization

The mesostructuration of amorphous oxides, followed by crystallization has been studied in depth and is well-understood. The self-assembly during evaporation occurs through complex interactions between solvent, precursors and template species, which can be described using free energy terms.[125] Free energy terms for molecular interactions between organic-inorganic species (ΔG_{inter}), organic-organic species (ΔG_{org}), inorganic-inorganic species (ΔG_{inorg}) and the solvent (ΔG_{sol}) all contribute to the organization within the solution (Eq 1):

$$\Delta G = \Delta G_{inter}\,(A, \rho_{inor}, \rho_{org}\ldots) + \Delta G_{org}\,(A, \rho_{inor}\ldots) + \Delta G_{inorg}\,(\rho_{inor}) + \Delta G_{sol} \qquad (\mathbf{1})$$

As portions of the free energy terms are dynamic, depending on the species' charge distribution and physical state (ρ), and as the inorganic species polymerizes and the solvent evaporates, the organization will also evolve. Templates are typically block copolymers (*e.g.* Pluronics) or molecular surfactant species (*e.g.* Brij, CTAB), with the requirement that a hydrophobic tail is attached to either a polar head having area (*A*) which can interact with the inorganic species. In the case of Pluronics and Brij, the polyethylene oxide (PEO) block is likely complexing the inorganic species. There is some evidence that Ti(IV) acts to crosslink the PEO micelle shell.[126] As the Pluronics are bitailed surfactants the ΔG_{org} becomes a more important factor due to the van der Waals interactions that give additional stability to the formation of micelles. The hydrophobicity of the tail plays a significant role in micelle formation.[127] Micelles may be preformed in solution, or formed when the critical micelle concentration is reached during solvent evaporation, though in all cases with EISA, coorperative templating occurs and the structural organization evolves during drying. Evaporation rate is of course very important because it determines how much time the solutes have to organize and, in the capillary deposition regime, how much material is deposited.[128] The condensation of metal oxides usually takes several minutes to complete and aging under the appropriate conditions can significantly improve the periodicity of the film.[84,127] This rearrangement is due to the decrease in the charge of the species during condensation [129] and the equilibrium water content dissolved in the film and in the air. However the evaporative conditions during the deposition also play a strong role. Thus evaporation rate is controlled using temperature, humidity and solvent volatility.

The crystallization of amorphous mesostructured films has a major drawback, which is that crystallization and/or sintering can destroy the pore structure.[100] The wall:pore ratio is important. It was shown that a cubic pore structure, with walls of 10-12 nm was able to crystallize and maintain porosity where the 2D-hexagonal pore structure with walls of 7 nm

degraded at the onset of crystallization.[84] In order to create thicker walls, it is possible to lower the template:inorganic precursor ratio by changing the solvent.[96] When pentanol or butanol is used instead of ethanol, the cmc for most ionic and nonionic surfactants is lowered and thus less organic matter can be used to produce porous structures with thick walls, which can in turn be crystallized without structural degradation.

During thermal treatment, the volume of the metal oxide contracts as organization of the crystal lattice takes place. In an organized porous thin film, the pores are also contracted, however not uniformly leading to anisotropic mesoporosity (Figure 3).[56] The anisotropy arises from the attachment between the thin film and the substrate. Many substrates are already crystalline, thus no significant structural rearrangement is expected during thermal treatment and the substrate will hold the form of the structure in the *x,y*-plane, forcing contraction to occur almost exclusively in the *z*-direction. The distortion of the matrix during calcination and the dimensions of the ellipsoidal pores has been studied for alumina going from amorphous through different crystal phases using GI-SAXS and ellipsometric porosimetry.[56] The accessibility, organization and interconnectivity of mesopore structures are maintained in Al_2O_3 throughout the crystallization. This contraction, combined with structural reorganization during calcination can lead to the formation of nanopillar pore structures as pore openings merge and walls densify.[51,98]

Figure 3. Contraction of Al_2O_3 films during calcination to produce crystalline anisotropic fcc mesopores. The figure is partially reproduced with permission from images appearing in reference 56.

An in depth investigation of the kinetics and thermodynamics of crystallization in mesoporous and dense TiO_2 thin films has been carried out using *in situ* thermal ellipsometric analysis.[130] The transition from amorphous to crystalline titania leads to first an increasein refractive index (RI) from 2.00 to 2.35 at the wavelength of 700 nm in dense films. Porosity

decreases the refractive index due to the contribution from air, but the same increase in RI is observed. Upon continued heating, decreases in refractive index are then observed, correlating to an increase in porosity due to pore coalescence during TiO_2 densification. The effect of heating rate, humidity, solution aging, film thickness, substrate dilatation coefficients, mesopore order and acidity on crystallization were all examined (Table 2). Highly ordered films, such as the cubic mesopore structure, showed decreased diffusion of TiO_2 than poorly ordered or dense films, leading to higher energy barriers to crystallization and crystal growth in the ordered film. However, highly crystalline and porous films were obtained upon heating to higher temperatures (630 °C in this case). This work proved also that, as opposed to dense films, a film exhibiting a well ordered mesoporosity made of TiO_2 domains of similar size. The result of this monodispersity in nanocrystals is that the resulting films present a very good thermal stability due to limited Oswald ripening during crystal growth. Mesopores affect crystallization by increasing the surface energy, adding capillary stresses due to the high-curvature of the pores (thus more effectively occluding water, templates and residual carbon) and confining the growth of nanocrystals.

Table 2. Summary of parameters and their effect on calcination and final film processes (↑, small increase; ↑↑, large increase; ↑↑↑, extremely large increase; NC, no change). T_{cryst} is the onset temperature of crystallization, where T_{pyr} is the temperature of pyrolysis in inert gas. Table reproduced with permission from reference 130.

	dense films		mesostructured films		
	crystallization	final density	calcination	crystallization	final density
increasing heating rate	↑↑ $T_{cryst.}$	↑↑	↑↑ $T_{pyr.}$	↑↑ $T_{cryst.}$	↑↑
increasing H_2O during calcination	↓↓ $T_{cryst.}$	↓↓	NC[a]	↓↓ $T_{cryst.}$	↓↓
increasing solution aging	↑ $T_{cryst.}$	↓	NC	NC	↓
decreasing film thickness	↑ $T_{cryst.}$	NC	NC	NC	↑
substrate	various	various	various	various	various
increasing mesostructure order			NC	↓ dim.[b]	
HCl vapor			↓↓ $T_{pyr.}$		↓↓↓

[a] T_{pyr} is higher for materials calcined under argon due to the absence of O_2.
[b] Change in mechanism resulting in an observed reduction of dimensionality in kinetically governing transport processes.

To summarize, the morphology of the mesopores affects the crystallization behavior, changing the onset of crystallization temperature, the crystallite size and even the crystal phase. Processing (choice of surfactant, substrate, solvent, chemical ratio, evaporation rate, deposition conditions, post-deposition treatment, etc.) can be used to master control over the morphology, which will in turn impact the crystallization dynamics. Some inorganic precursors can crosslink the shell of some micelles, freezing the micelle morphology even before micelle packing on the substrate during film drying. During heat treatment, the inorganic species will densify and undergo diffusive sintering, limited by the pore structure of the film, the heat treatment time and temperature. During densification, the film shrinks anisotopically, as the attachment to the substrate prevents significant contraction parallel to the wafer. Thus the substrate, processing conditions and mesostructure are all interrelated with final crystallinity.

IV. Nanostructuration of crystallized particles

Nanostructuration followed by crystallization is an excellent method for most materials. However, the formation of nanocrystals followed by mesostructuration by dip-coating the sol with appropriate block copolymers has proven to be desirable for the formation of doped materials, such as Nb doped TiO_2 and Sb doped SnO_2.[38,131] Pre-crystallization avoids collapse of the mesostructure upon crystallization and thermal degradation of the templates.[132-134] This route is also interesting for applications where control over particle size is paramount or when the substrate is temperature-sensitive.[135] In pure titania, primary particles of 2-8 nm of anatase and brookite are formed and agglomerate through standard sol-gel chemistry, followed by dissolution of larger aggregates via peptidization. These nanobuilding blocks are then assembled around micelles during deposition onto a substrate.[136] The main benefits include control over particle size and doping, as these are often linked to the calcination program. The calcination program is in turn at least partially dependent on the decomposition temperature

of the templates. However, to successfully mesostructure the film, the crystalline particles must be significantly smaller than the micelles, with narrow particle size distribution, and should be well dispersed in the relevant solvents. Also the temperature and aging time of peptidization must be precise to control the colloid size.[137]

For example, some titania nanocrystals can be formed from $TiCl_4$ in dry organic solvents by heating to 80 °C for 9 h in a loosely sealed vessel.[132] The titania sol was combined with amphiphilic KLE block copolymers and dip-coated to produce mesoporous thin films. The same block copolymers were used with titanium precursors under standard EISA conditions to compare the pre- and post-crystallization methods. Anatase appeared in the post-crystallized film at 500 °C with 100% crystallinity occurring by 600 °C. In the pre-crystallized film, anatase grain growth could be observed from the decomposition temperature of the template (400 °C) up to 900 °C. The presence of rutile was not observed in either film. The significant difference between the films prepared via pre- and post-crystallization was that pre-crystallized films demonstrated crystallographically oriented nanocrystals, albeit with a low degree of orientation, whereas the post-crystallized titania leads to completely random orientation for all reported substrates.

Although it looks very simple, this approach requires the use of small nanocrystals presenting a high surface reactivity which makes the unraveling of real film formation mechanism not always straightforward. For example, in a study of mesoporous mixed ZrO_2-TiO_2, it was found that nanocrystalline building blocks were either formed in solution or in the initial drying of the film, which degraded into a mixed amorphous oxide upon aging in a humid environment.[127] The higher the %RH, the faster the nanocrystals degraded. The degradation of the crystalline structure coincided with the growth of a mesoporous phase, indicating that nanobuilding blocks perhaps act as a feed stock rather than as nanobricks around a porogen.

Ceria is a material that often suffers from mesopore collapse upon crystallization.[134] Ceria sols were prepared by precipitating ammonium cerium nitrate in basic pH, followed by peptidization in 1:1 H_2O:HNO_3.[138] Colloidal ceria was assembled into 3D mesostructured films by using crystalline sols. Mixtures of ethanol, water, amphiphilic block copolymer (poly(hydroxybutyrate)-poly(ethylene oxide), PHB-PEO) and ceria nanoparticles (~3 nm) were deposited using dip-coating. The ethanol:water ratio was critical as in highly aqueous media the gelation of particles occurred faster than the structuration process. Only very specific synthetic conditions allowed the formation of highly ordered, porous and crystalline thin films with mesopores of ~11 nm separated by a double layer of particles, that is walls of 6-7 nm.

Ortel, *et al.* did a comparative study between the assembly of nanobuilding blocks and $TiCl_4$ around laboratory-made block copolymers.[32] Compared to the precursor, the use of NBBs generated pore structures that were less well-defined, due to the difficulty assembling the preformed nano-objects around the micelles. The NBB approach produced a high degree of roughness that increased surface area substantially. As could be intuitively predicted, when NBBs are used instead of $TiCl_4$, the anisotropic film shrinkage (Figure 4) is much less pronounced. For instance, calcined films produced from PEO_{213}-PB_{184}-PEO_{213}-$TiCl_4$ had final pore dimensions of 21 x 5 nm, where the PEO_{213}-PB_{184}-PEO_{213}-NBB system had pore dimensions of 17 x 13 nm. Thus shrinkage in films produced from NBBs is more homogeneous in all 3 dimensions.

Figure 4. Top-view SEM images at low and high magnification of PEO_{213}-PB_{184}-PEO_{213} templated titania films prepared using (a, b) $TiCl_4$ and (c, d) TiO_2 NBBs. The figure is reproduced with permission from images appearing in reference 32.

Hartmann, et al. compared the photoelectric properties of mesoporous titania thin films prepared via EISA of surfactants and $TiCl_4$ and pre-formed TiO_2 NBBs.[139] The films prepared from NBBs had twice the surface area, and a more accessible surface due to larger pore openings. However, the quantum efficiency (incident photon capture efficiency, IPCE) was an order of magnitude higher for the sol-gel films. The explanation for this unexpectedly high photon conversion efficiency in the sol-gel derived film is that there is a lower fraction of grain boundaries and more direct electron pathways than in the film constructed from NBBs.

V. Surfactant mediated iso-oriented crystals and mesopore morphology

Surfactants are able to induce both crystallite and pore alignment. They play a role in determining the morphology, pore accessibility, diffusion and performance in applications. Oriented pore arrays may be obtained by surfactant-substrate interactions,[140] photo-induced polymer orientation,[141] sheer flows[142] and magnetic processing,[17] but also can be formed by mastering surfactant assembly dynamics. The physicochemical interactions between surfactant and inorganic precursors/particles should therefore be understood in detail.

The EISA generation of porous oxides uses a non-expensive methodology stemming from depositing a solution of block copolymers or surfactants and inorganic precursors on a substrate. The micelles interact with the substrate regardless of its hydrophilic or hydrophobic character due to their amphiphilicity. However, the resulting pore morphology depends upon the micelle-substrate interaction.[143-144] In the case of hydrophilic substrates, favorable interactions with the micelle may be obtained through hexagonal pore arrays lying in the plane.[140] When the substrate is hydrophobic, hemi-micelles deposit on the surface.[140,145] In an interesting example, poly(hexamethylenepyromellitimide) (PI) was used as a substrate because it has an anisotropic structure that can be aligned in a particular direction with rubbing.[146] Micelles of long chain surfactant aligned themselves with the PI interface, which

elongated the micelle spacing and drastically changed the crystallographic orientation of the hexagonal mesostructured silica formed there from.

Vertical pore arrays may be desirable so that the channels that exist connect the solution to the substrate via the film,[57,147] and because they can generate anisotropic photoluminesce.[148] This morphology is typically not observed because other available structures are energetically more favorable. However, vertical pores have been obtained by using a patterned surface (Figure 5).[149] The patterned surface was deposited by coating the substrate with a cubic pore organization in titania, which presents hexagonal morphology on the top layer. A second hexagonal phase was then deposited using silica, this time with hexagonal pores running vertically. To obtain a good match between the titania and silica lattices, pitch was tuned through either a careful selection of block copolymer templates, or through swelling the hexagonal pore templates with non-polar solvents. The formation of the hexagonal layer must be kinetically slow so that there is time for the micelles to arrange on the patterned substrate, thus explaining the use of silica as the second layer. The authors of this study noticed that close to the substrate, the epitaxial interactions are strong and can force organization even when the lattice match is rather poor with disorder becoming more apparent with distance from the substrate (Figure 5c).

Figure 5. (a) Graphical depiction of epitaxial growth of hexagonal silica films on cubic TiO_2. Micrographs of hexagonal SiO_2 grown above cubic TiO_2 with a (b) good and (c) poor lattice match. The figure is reproduced with permission from images appearing in reference 149.

Two additional routes to obtaining vertical pore alignment have been reported. The first uses patterned substrates that induce a particular surfactant assembly (e. g. a conical shape drilled into the substrate), that then propagates vertical pore alignment through the film thanks to epitaxy.[150-151] The second consists of using π- π interactions between the template and the

substrate, as was obtained through assembly of liquid crystalline arrays of conjugated polyaromatic compounds interacting with a highly oriented pyrolytic graphite wafer.[152] Although these reports concern the formation of amorphous silica,[150-152] other oxides that crystallize via calcination could be performed with vertical mesopores through this technique.

Surfactants have been used to mediate the oriented nucleation of crystallites with anisotropic unit cells, including MoO_3, Nb_2O_5, Ta_2O_5, $TaNbO_5$, V_2O_5 and $LiTaO_3$ (Figure 6).[76,153] These crystallites have uniaxial oriented nanocrystals relative to the substrate with crystallite size and orientation coupled to the mesostructure.[76] The crystal orientation is determined from the onset of nucleation. The pronounced epitaxial relationship can be ascribed to the directional van der Waals force, acting upon the crystallites which have alternating oxygen- and metal-rich sheets normal to the long b-axis (Figure 6b). The polarization of the anisotropic unit cell thus maximizes van der Waals attraction to the surface by aligning in the orientation shown in Figure 6b. For a reason not clear yet, the presence of surfactants lowers the crystallization temperature as compared to bulk matter.[76] In fact, when thermal energy (kT) is too high, random grain growth results, indicating the delicate contribution of mesostructuration to crystallization kinetics. Surfactants may also increase the surface mobility of species due to lubrication.[153] At high surfactant concentration mesoporosity was observed and at low surfactant concentration a dense film was produced, but in both cases the oxide had epitaxial orientation. Perhaps the degradation of the surfactant leaves residual carbon as a barrier layer between the film and the substrate, thus allowing the van der Waals forces to act without competing effects from the epitaxial relationship with the substrate.[76] This surface passivation might explain why iso-oriented crystals are observed on virtually any substrate.[76] Moreover, the size of the crystallite was larger (40-45 nm) than the mesopore spacing (~15 nm),[73] generating mesopore arrays with straightened walls and

elongated nanocrystals. The distinct shapes of the crystallites and of the mesopores mean that the crystallization did not affect the mesostructuration.

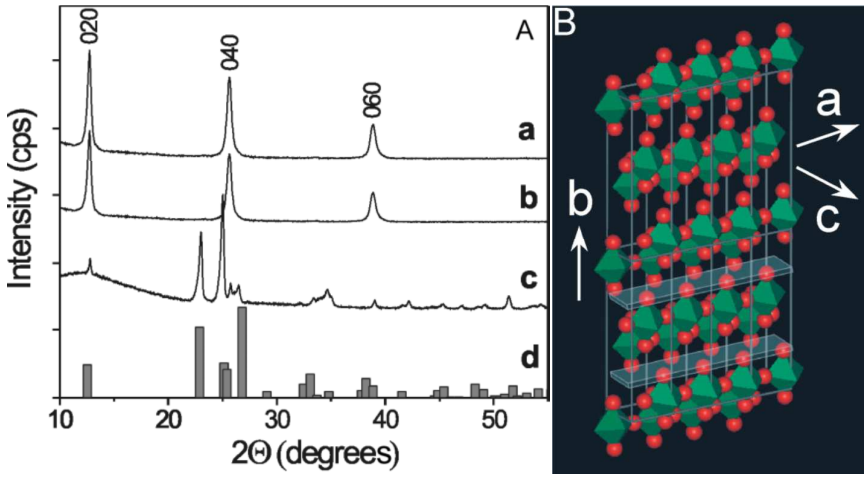

Figure 6. A. XRD analysis of non-porous and mesoporous crystalline MoO_3 films on glass substrates, (a) 25 wt% surfactant, (b) 0.03 wt% surfactant, (c) no surfactant, (d) JCPDS database pattern 5-508. B. Illustration of the molybdite unit cell composed of Mo (green) and oxygen (red). The figure is reproduced with permission from images appearing in reference 153.

VI. Substrate-directed crystallization.

The crystallinity of a thin film can be affected by the crystal lattice of the substrate on which it is deposited. The substrate can transfer its epitaxy, residual stresses and strain to the thin film, and the interfacial energies between the film and the substrate also affect crystallization behavior. Another point to note is that sometimes the substrate will react chemically with the deposited film, requiring a buffer layer to keep the oxide from becoming contaminated. The substrate additionally plays a role in wetting and cracking of the deposited film, as discussed previously.

Mesoporous titania films were deposited on Si(111), a single crystal Pt and glass substrates.[154] Heat treatment at 350 ºC led to enhanced anatase crystallinity for the films deposited on the Si(111) wafer, followed by the Pt substrate, as compared to that deposited on amorphous glass.[154] This trend is explained by the fact that the crystalline structure of the substrate may offer heterogeneous nucleation sites, lowering the nucleation energy barrier. In line with this thinking, a comparison of the luminescence band intensities of these TiO_2 films showed that the film deposited on Si(111) exhibited a higher density of surface defects (*e.g.* oxygen vacancies), whereas that deposited on Pt contained more interstitial Ti^{3+} sites.

A XANES study of the crystallization behavior of anatase on ITO and Si substrates found that only 50% of the thin film was crystalline on ITO after heat treatment at 500 ºC for 1 h.[91] By contrast, 90% of the thin film was crystalline upon heat treatment at 350 ºC when a silicon substrate was used instead. The authors hypothesize that cations from ITO supported on glass migrate into the TiO_2 film and stunt crystal growth through glasslike shells around growing particles. Supporting this point, a buffer layer of titania in between an ITO substrate and a mesoporous titania layer resulted in crystallization under conditions where a mesoporous coating without the buffer layer was amorphous.[92] Additionally the authors probe the photocatalytic activity after different thermal treatments to show what happens with the actual properties even before extensive crystallization.[91]

Two crystallization studies have been conducted, one about nickel containing TiO_2,[155] and one about $Bi_2VO_{5.5}$,[156] on Si(100) containing a native layer of SiO_2 and after SiO_2 removal with HF. In both cases the substrate containing the native SiO_2 layer produced a more crystalline film than the stripped Si(100) substrate. In fact, the amorphous to crystalline phase transition occurred 150 ºC lower when the native SiO_2 layer was present.[155] The substrate effect is attributed to the mismatch in the lattice constant between the thin film and the Si(100), which is decreased upon the incorporation of a SiO_2 buffer layer. Moreover, the

degree of Ni^{2+} incorporation into the TiO_2 matrix was affected as apparently Ni^{2+} has differing solubility in anatase and rutile.[155] As the substrate affected the anatase-rutile transition, it also affected the homogeneity and the temperature of incorporation of Ni^{2+} into the matrix.

VII. Epitaxial quartz films

Once the organic precursors are decomposed during the thermal treatment, the substrate can act as a template for epitaxial growth. Therefore, substrates are a key component when growing high quality crystalline films. In this direction, it is important to select a proper substrate in concordance with the crystallographic characteristics and goals of the nanostructured crystalline films.

There are some points to consider when choosing a substrate, including chemical compatibility with the structure to be grown, thermal expansion coefficients and thermal stability during the growth process.[157] In addition, the lattice mismatch between structures is an important factor to take into account for epitaxial growth, which requires growing in a controlled crystallographic orientation.[158] Thus, by considering all these contributing factors, it is possible to generate different nano-architectures by using the epitaxial relationship between similar crystallographic structures to advantage during the growth process. This growth mechanism permits soft chemistry to extend an oriented epitaxial growth to a variety of functional oxide nanostructures.[157,159-161]

Harnessing the epitaxy of the substrate to induce oriented crystal growth in another material can allow preparation of functional materials that are otherwise inaccessible. For example, *A. Carretero-Genevrier et al.* used silicon substrates to develop structured epitaxial piezoelectric quartz thin films (low α-quartz).[25,162] These films were obtained through the EISA of a sol-gel solution dip-coated onto Si(100) substrates. The sol-gel solution contained partially hydrolyzed and condensed tetraethoxysilane (TEOS) as a quartz precursor. The quartz

thickness was defined by the thickness of the amorphous film deposited and by the calcination conditions, allowing the generation of films much thinner than previously generated (10 μm minimum).[163] The silica precursor solution contained a specific proportion of Sr^{2+}, Ba^{2+} or Ca^{2+}, incorporated as nitrate or chloride salts, which functioned as silica network modifiers.[164-166] A homogeneous distribution of these alkaline earth metals within the amorphous silica allowed for the heterogeneous nucleation of crystalline quartz of sufficiently small crystallite size so as to preserve large mesostructures present within the amorphous films. The devitrificants Sr^{2+}, Ba^{2+} and Ca^{2+} can either be included in the film *in situ* (Figure 7) or during a secondary infiltration (Figure 8), in both cases allowing for crystallization at relatively low temperatures.[25] In this straight-forward approach, the low mismatch between the (100)-quartz plane and the crystalline (100)-silicon substrate induces the nucleation of α-quartz crystals at the silicon-silica interface during thermal treatment above 900 ºC (5 hours in air at ambient pressure). As a consequence, the formation of an oriented polycrystalline α-quartz thin film is epitaxially selected by the crystallographic orientation of the (100)-silicon substrate. When the same protocol was applied to particles not in contact with a crystalline substrate, there was no orientation to the crystal planes.[167] Moreover, the authors show that other polymorphs of silica do not exhibit a comparable mismatch with the silicon substrate, thus avoiding the stabilization of other crystalline silica phases during the thermal treatment (Figure 7).

Figure 7. Scheme of the formation of an oriented polycrystalline α-quartz thin film with epitaxially selected crystallographic orientation from the (100)-silicon substrate by the one-pot route. 1) Cross-section of the original mesoporous film showing homogeneous Ba^{2+}, Sr^{2+} or Ca^{2+} distribution within the amorphous silica matrix. 2) Nucleation above 900 ºC of α-quartz crystals at the silicon-silica interface during the devitrification of the original amorphous mesoporous film. 3) Oriented columnar quartz crystallite growth within the original (100)-silicon substrate, where crystallization rate and depth is limited by oxygen diffusion. HRTEM image of the α-quartz-Si interface along [001] exhibits the crystallinity of quartz on silicon. The melting agents (Ba^{2+}, Sr^{2+} or Ca^{2+}, blue spheres), used to devitrify amorphous silica, migrate from the interior of the film during quartz formation, to the crystal boundaries. The figure is reproduced with permission from images appearing in reference 25.

Figure 8. Scheme of the formation of an oriented polycrystalline α-quartz thin film with epitaxially selected crystallographic orientation from the (100)-silicon substrate by infiltration of network modifiers into the mesoporous SiO_2. Top-view and cross-sectional SEM images of the amorphous mesoporous silica films (left) were infiltrated with Ba^{2+} or Sr^{2+} (center). Nucleation above 1000 ºC of α-quartz crystals at the silicon-silica interface during the devitrification of the amorphous silica generates oriented columnar quartz crystallite growth while preserving the mesostructure in the upper quartz layer (right).

The evolution of individual quartz crystallite sizes, morphology, and orientation is driven by an oriented competitive growth mechanism that mediates a preferential orientation of quartz crystal nuclei and produces a columnar microstructure. During this singular

competitive growth process, crystal aggregates with the orientation imposed by the (100)-silicon succeed over those that do not have such orientation (See Figure 9).

Figure 9. (a) FEG-SEM micrograph displaying a cross-sectional view of the oriented columnar microstructure in a quartz thin film. (b) A 3D model of the in-plane epitaxial relationship between the quartz film (in orange) and the silicon substrate (in gray) viewed along the [011] zone axis. (c) XRD θ-2θ scan of an epitaxial quartz film that shows the diffraction pattern in the (100) crystallographic direction. The figure is reproduced with permission from images appearing in reference 25.

This particular oriented competitive growth mechanism was coupled together with the flexibility of soft chemistry to master control over different pore domains in quartz thin films. The use of templating agents such as surfactants, PB-PEO diblock copolymers or phase separation allowed for the first preparation of piezoelectric mesoporous and macroporous quartz films (Figure 10). Large pores (>25 nm) are then retained upon crystallization but small ones (<25 nm) collapse, leading to dense α-quartz films.[25-26] These results suggest that a minimum curvature close to 0.08 nm^{-1} can be accommodated by the α-quartz crystals, though the wall thickness is apt to also play a role. Thus, in Figure 10 we can see that the original d-spacing does not apply to the crystallized sample and diffusive sintering has occurred. Typically, mesopore structures are lost during the crystallization of silica due to the relatively slow nucleation rate followed by the extremely fast growth rate of quartz,[168] which generates crystallites much larger than the original pore structures. Thus previous to this report in 2013,[25] the only way to access structured quartz was through the use of physical techniques with a limited size domain.[169-170]

Figure 10. Schematic of heteroepitaxial growth of α-quartz thin films on Si(100) from silica films deposited using sol-gel chemistry. (a, c, e) FEG-SEM images demonstrating the different pore size obtained in amorphous silica films: macroporous and mesoporous with an average pore of (a) ≈ 700 nm, (c) ≈ 28 nm and (d) ≈ 2 nm. (b, d, f) AFM images display the crystallized nanostructured quartz thin films with the different pore sizes. The figure is partially reproduced with permission from images appearing in reference 25.

In addition to standard templating techniques, material scientists can now make use of a new phase separation technique to generate macropores of controllable size between 75-2000 nm.[26] The films are prepared using dip-coating with the devitrificant salts present in solution (Figure 11). Although many salts can be used for the phase separation process, so far only Ca^{2+}, Sr^{2+} and Ba^{2+} have led to the crystallization of quartz under the concentrations of melting agent and thermal treatment conditions tested.[25-26]

Figure 11. Scheme of macroporous (700 nm) epitaxial quartz crystallization *via* phase separation. (a, b) The phase separation mechanism is followed by a swift deweting process, where ions of strontium or calcium were homogeneously confined within the amorphous silica matrix during gelification and drying of dip coated films. (c) This process enables quartz thin films to keep the initial template arrangement and pore size as obtained during phase separation at room temperature. The figure is partially reproduced with permission from images appearing in reference 26.

Although many glasses contain the network modifiers used to crystallize SiO_2, crystallization in thin films was not previously observed under such mild conditions. We have observed that oddly an excess of devitrificant prevents crystallization. One possible

explanation is that at higher concentrations of network modifiers, ion mobility is decreased.[171] Only catalytic quantities lead to epitaxial growth. A deficit of melting agent causes non-oriented crystal growth and large proportions of amorphous material (Figure 12).

Figure 12. Thermal treatment at 1000 ºC of macroporous silica films prepared using different contents of Sr^{2+} relative to 16.3 mmol Si. (a) XRD pattern of samples with 0.25 (green), 0.5 (blue), 1 (red), and 2 (pink) mmol of Sr^{2+}. FEG-SEM images of (b, c) 2 mmol of Sr^{2+}, (d, e) 1 mmol of Sr^{2+}, (f, g) 0.5 mmol of Sr^{2+}, (h, g) 0.25 mmol of Sr^{2+} relative to 16.3 mmol Si. The figure is partially reproduced with permission from images appearing in reference 26.

Irrespective of the pore size, the piezoelectric functionality of the quartz films is completely preserved (Figure 13). We show that piezo-response force microscopy response (PFM) preserves the features of the topographic image, namely the boundaries between the crystals surrounding the porosity and the perimeter of the pores, with no significant differences between the PFM response in the inner and outer regions of the pore.[26] Thus, the authors demonstrated that the combination of soft chemistry and epitaxial growth opens opportunities for the controlled design of textured crystalline solids attractive for further integration of functional oxides onto silicon substrates.

Figure 13. Piezoelectric response of macroporous epitaxial quartz films. (a) AFM image of the topography, and (b) the PFM amplitude recorded simultaneously under a tip-substrate AC voltage of 10 V. (c) The amplitude response to different applied tip voltages. This figure is reproduced with permission from reference 26.

In this light, *Carretero-Genevrier et al.* used these recent developments of soft chemistry based routes to integrate α-quartz thin films on silicon substrates for the epitaxial growth of single crystalline oxide nanowires films.[172] The nucleation and crystalline growth of 1D nanostructures were observed on silicon substrates when Sr^{2+} or Ba^{2+} cations were present in the precursor solution. Once again, Sr^{2+} or Ba^{2+} cations induced a heterogeneous catalysis that allows the devitrification of the native amorphous surface layer to finally obtain the crystallization of α-quartz crystals at the interface. This polycrystalline α-quartz film renders the convenient interface lattice matching to the complex oxide nanostructures for the epitaxial growth of manganate nanowires (OMS) at 800 °C (Figure 14).

Figure 14. Schematic of the stages of the crystallization process for single crystalline manganates OMS nanowires on silicon. (1) Track-etched nanoporous polymer template supported on a SiO_2/Si substrate filled with the chemical precursor solution allowing a homogeneous distribution of Ba^{2+} or Sr^{2+} melting agents. (2) At mild temperatures (500-600 °C) confinement nucleation in high aspect ratio nanopores of seed nanowires. (3) Devitrification of the SiO_2 layer and nucleation of α-quartz takes place at the interface where epitaxial growth of mangantes OMS nanowires on the quartz is promoted at high temperatures (800 °C). This figure contains images that are reproduced with permission from 26.

This innovative methodology involves the use of track-etched nanoporous polymer templates combined with the growth of quartz thin films as described elsewhere.[173] Significantly, this confined growth mechanism is extendable to different NW compositions, as long as Ba^{2+} or Sr^{2+} are present in the initial nanowire precursor solution as devitrifying agents. Thus, authors obtained by chemical solution deposition the synthesis of different

single crystalline epitaxial nanowires films, including $Ba_{1+\delta}Mn_8O_{16}$ hollandite, $Sr_{1+\delta}Mn_8O_{16}$ strontiomelane, $(BaSr)_{1+\delta}Mn_8O_{16}$ and a novel crystallographic phase named LaSr-2×4 OMS on top of (100)-silicon substrates (Figure 15).[172] The LaSr-2×4 OMS nanowires display enhanced ferromagnetic properties with a Curie temperature higher than 500 K,[174] and $Ba_{1+\delta}Mn_8O_{16}$ hollandite nanowires show a ferromagnetic ordering at low temperatures (~40 K).

This work marks the importance of a good interplay between chemical compatibility, lattice mismatch, crystallographic structure, interface, and surface energies which is fundamental for nanostructure nucleation and further crystallographic phase stabilization.[175]

Figure 15. Schematic depicting the steps in the upper figures from the polymer template filling with the precursor solution at RT to the nanowire formation at 800 °C. Low magnification and high magnification (as insets) images of the final OMS nanowires obtained, i.e (a) La-Sr-Mn precursors (LaSr-2×4 OMS), (b) Ba- Mn-precursors ($Ba_{1+\delta}Mn_8O_{16}$), (c) Sr- Mn-precursors ($Sr_{1+\delta}Mn_8O_{16}$) and (d) Ba- Sr- Mn-precursors ($(BaSr)_{1+\delta}Mn_8O_{16}$). This figure is reproduced with permission using some images that were previous published in reference 175.

VIII. Outlook and Conclusions

In this manuscript, we highlighted the most successful synthetic strategies used currently to fabricate structured nanocrystalline thin films. The majority of research has focused on optimizing synthetic strategies to obtain the best properties from the nanocrystalline films for various applications of high societal impact. After about sixteen years of development, almost any type of simple or complex metal oxide can be obtained as a structured thin film, either by

direct crystallization onto a substrate or by post deposition of crystalline nanoparticles. The main physico-chemical understanding of crystallizing structured systems has been explored in this review, with explanation of the importance of substrate-film interfacial energies, micelle-substrate interactions, and how micelle structure can orient crystal growth due to unit cell alignment with micelles due to van der Waals interactions. The mesostructuration increases the interfacial energy and thus typically lowers crystallization temperatures. Also considered are the complex and dynamic chemistry of EISA film deposition, the contraction stresses of structured materials during crystallization, and the colloid-micelle interactions when NBBs are used. Crystalline mesoporous metal oxides can be formed with a high degree of control over 2D and 3D architectures. Future research should focus on fully decoupling crystallinity and pore structure and extending the applications of these films.

Most commonly, crystallization requires pressure and/or heat to convert the amorphous network into a regularly structured framework. These conditions preclude the creation of a hybrid material, eliminating large domains of application. “Crystal like” hybrid materials were reported which relied on H-bonding, hydrophobic-hydrophilic interactions and π-π stacking in order to “crystallize” around an ordered mesoporous structure.[176] There is vast potential for hybrid crystalline thin films in applications which rely upon conduction, thermal stability, mechanical strength, low density and tunable micro- and mesoframeworks and thus we hope to see vast developments in this area of research.

We have shown the power of coupling the epitaxial relationship of the substrate and the film with soft chemistry.[25-26,167] This fusion of physics, chemistry and processing allows structured, oriented crystalline thin films to be produced through chemical solution deposition, via a straightforward, reproducible and commercially applied dip-coating process. Complex materials such as these films can thus open up new applications for biological sensors and piezoelectric resonators with higher sensitivities than current state of the art.

Moreover, these structured piezoelectric responsive films can be used as substrates to grow antenna displaying a magnetic or an electronic field, opening the doorway to new optical and electronic devices. Further research in the domain should focus on further understanding the crystallization mechanism, measuring the Q-factor of these ultra thin mesoporous resonators, increasing the complexity of quartz architectures and integrating these piezoelectric structured films into devices.

Although some successful industrial applications have been reported, the real societal impact of such thin films is still limited by a lack of practical development of their integration in industrially functional systems. The industrial application constrains typically arise from: (i) *The substrate on which the thin film must be deposited*. One often meets substrate chemical and thermal stability, or thermal expansion coefficients incompatible with the thermal treatment needed for the crystallization or the stabilization of the nanocrystalline layer. (ii) *The industrial deposition processing* must be adapted to both the solution chemistry and the geometry of the substrates. For instance current challenges include, high speed deposition onto large flat panels, 3D deposition onto substrates with complex or tortuous geometries, and precisely controlled liquid deposition on small surfaces for integration of microsystems. (iii) *The in operando stability of the properties and integrity of the nanocrystalline layers* are eventually always critical parameters. As these critical points are scarcely discussed in the literature, the actual prospects of evolution is obviously to accelerate the development of industrially compatible liquid deposition and stabilization processes that can directly impact the economic viability, stability and potential toxicity of the nanocrystalline thin films.

Acknowledgements

ACG and GLD acknowledge Collège de France foundation and Solvay for material and financial support and IMPC for use FEG-SEM facilities. Additional finances were provided to A.C.G by the project PEPS Cellule Energie de l'INSIS-CNRS (1D-RENOX). ACG

acknowledges Collège de France and LCMCP for his Visiting Scientist position and INL-CNRS for his detachment. We thank David Montero and Mohamed Selmane for technical support.

References

(1) Drisko, G. L.; Sanchez, C. *European J. Inorg. Chem.* **2012**, *2012*, 5097.
(2) Faustini, M.; Drisko, G. L.; Letailleur, A. A.; Montiel, R. S.; Boissiere, C.; Cattoni, A.; Haghiri-Gosnet, A. M.; Lerondel, G.; Grosso, D. *Nanoscale* **2013**, *5*, 984.
(3) Franceschini, E. A.; Planes, G. A.; Williams, F. J.; Soler-Illia, G. J. A. A.; Corti, H. R. *J. Power Sources* **2011**, *196*, 1723.
(4) Liang, C.; Hong, K.; Guiochon, G. A.; Mays, J. W.; Dai, S. *Angew. Chem., Int. Ed.* **2004**, *43*, 5783.
(5) Fischereder, A.; Martinez Ricci, M. L.; Wolosiuk, A.; Haas, W.; Hofer, F.; Trimmel, G.; Soler-Illia, G. J. A. A. *Chem. Mater.* **2012**, *24*, 1837.
(6) Vinu, A. *Adv. Funct. Mater.* **2008**, *18*, 816.
(7) Gu, D.; Schüth, F. *Chem. Soc. Rev.* **2014**, *43*, 313.
(8) Soler-Illia, G. J. A. A.; Crepaldi, E. L.; Grosso, D.; Sanchez, C. *Current Opinion Colloid Interface Sci.* **2003**, *8*, 109.
(9) Nicole, L.; Boissière, C.; Grosso, D.; Quach, A.; Sanchez, C. *J. Mater. Chem.* **2005**, *15*, 3598.
(10) Li, W.; Yue, Q.; Deng, Y. H.; Zhao, D. Y. *Adv. Mater.* **2013**, *25*, 5129.
(11) Innocenzi, P.; Malfatti, L. *Chem. Soc. Rev.* **2013**, *42*, 4198.
(12) Ariga, K.; Vinu, A.; Yamauchi, Y.; Ji, Q. M.; Hill, J. P. *Bulletin Chem. Soc. Japan* **2012**, *85*, 1.
(13) Soler-Illia, G. J. A. A.; Azzaroni, O. *Chem. Soc. Rev.* **2011**, *40*, 1107.
(14) Soler-Illia, G. J. A. A.; Angelomé, P. C.; Fuertes, M. C.; Grosso, D.; Boissiere, C. *Nanoscale* **2012**, *4*, 2549.
(15) Vinu, A.; Mori, T.; Ariga, K. *Adv. Mater.* **2006**, *18*, 753.
(16) Faustini, M.; Drisko, G. L.; Boissiere, C.; Grosso, D. *Scripta Materialia* **2014**, *74*, 13.
(17) Yamauchi, Y. *J. Ceram. Soc. Jpn* **2013**, *121*, 831.
(18) Sanchez, C.; Belleville, P.; Popall, M.; Nicole, L. *Chem. Soc. Rev.* **2011**, *40*, 696.
(19) Jose, R.; Thavasi, V.; Ramakrishna, S. *J. Am. Ceramic Soc.* **2009**, *92*, 289.
(20) Shiju, N.; Raveendran, G.; Vadim, V. *Appl. Catal. A-Gen.* **2009**, *356*, 1.
(21) Sun, S.; Yang, Z. *RSC Adv.* **2014**, *4*, 3804.
(22) Takamasa, I. *J. Ceram. Soc. Japan* **2008**, *116*, 462.
(23) Antolini, E. *Solid State Ionics* **2004**, *170*, 159.
(24) Cui, J.; Gibson, U. *Phys. Rev. B* **2006**, *74*, 045416.
(25) Carretero-Genevrier, A.; Gich, M.; Picas, L.; Gàzquez, J.; Drisko, G. L.; Boissiere, C.; Grosso, D.; Rodriguez-Carvajal, J.; Sanchez, C. *Science* **2013**, *340*, 827.
(26) Drisko, G. L.; Carretero-Genevrier, A.; Gich, M.; Gàzquez, J.; Ferrah, D.; Grosso, D.; Boissiere, C.; Rodriguez-Carvajal, J.; Sanchez, C. *Adv. Funct. Mater.* **2014**, *doi 10.1002/adfm.201401066*.
(27) Drisko, G. L.; Luca, V.; Sizgek, E.; Scales, N.; Caruso, R. A. *Langmuir* **2009**, *25*, 5286.
(28) Yu, J. C.; Yu, J. G.; Ho, W. K.; Jiang, Z. T.; Zhang, L. Z. *Chem. Mater.* **2002**, *14*, 3808.
(29) Roncaroli, F.; Martinez, E. D.; Soler-Illia, G. J. A. A.; Blesa, M. A. *J. Phys. Chem. C* **2013**, *117*, 15026.
(30) Ide, A.; Drisko, G. L.; Scales, N.; Luca, V.; Schiesser, C. H.; Caruso, R. A. *Langmuir* **2011**, *27*, 12985.
(31) Li, Y.; Duan, G.; Liu, G.; Cai, W. *Chem. Soc. Rev.* **2013**, *42*, 3614.

(32) Ortel, E.; Fischer, A.; Chuenchom, L.; Polte, J.; Emmerling, F.; Smarsly, B. M.; Kraehnert, R. *Small* **2012**, *8*, 298.
(33) Sanchez, C.; Soler-Illia, G. J. A. A.; Ribot, F.; Lalot, T.; Mayer, C. R.; Cabuil, V. *Chem. Mater.* **2001**, *13*, 3061.
(34) Rozes, L.; Sanchez, C. *Chem. Soc. Rev.* **2011**, *40*, 1006.
(35) Sanchez, C.; Boissiere, C.; Grosso, D.; Laberty, C.; Nicole, L. *Chem. Mater.* **2008**, *20*, 682.
(36) Yoshitake, H.; Sugihara, T.; Tatsumi, T. *Chem. Mater.* **2002**, *14*, 1023.
(37) Hochbaum, A. I.; Gargas, D.; Hwang, Y. J.; Yang, P. *Nano Lett.* **2009**, *9*, 3550.
(38) Liu, Y.; Szeifert, J. M.; Feckl, J. M.; Mandlmeier, B.; Rathousky, J.; Hayden, O.; Fattakhova-Rohlfing, D.; Bein, T. *ACS Nano* **2010**, *4*, 5373.
(39) Li, Z.-X.; Shi, F.-B.; Ding, Y.; Zhang, T.; Yan, C.-H. *Langmuir* **2011**, *27*, 14589.
(40) Huang, Z.; Geyer, N.; Werner, P.; de Boor, J.; Gosele, U. *Adv. Mater.* **2011**, *23*, 285.
(41) Warren, S. C.; Messina, L. C.; Slaughter, L. S.; Kamperman, M.; Zhou, Q.; Gruner, S. M.; DiSalvo, F. J.; Wiesner, U. *Science* **2008**, *320*, 1748.
(42) Grosso, D.; Cagnol, F.; Soler-Illia, G. J. A. A.; Crepaldi, E. L.; Amenitsch, H.; Brunet-Bruneau, A.; Bourgeois, A.; Sanchez, C. *Adv. Funct. Mater.* **2004**, *14*, 309.
(43) Grosso, D.; Babonneau, F.; Albouy, P. A.; Amenitsch, H.; Balkenende, A. R.; Brunet-Bruneau, A.; Rivory, J. *Chem. Mater.* **2002**, *14*, 931.
(44) Soler-Illia, G. J. A. A.; Sanchez, C.; Lebeau, B.; Patarin, J. *Chem. Rev.* **2002**, *102*, 4093.
(45) Kirsch, B. L.; Richman, E. K.; Riley, A. E.; Tolbert, S. H. *J. Phys. Chem. B* **2004**, *108*, 12698.
(46) Reiner, J. W.; Kolpak, A. M.; Segal, Y.; Garrity, K. F. *Adv. Mater.* **2010**, *22*, 2919.
(47) Chambers, S. A. *Adv. Mater.* **2010**, *22*, 219.
(48) Brinker, C. J.; Lu, Y.; Sellinger, A.; Fan, H. *Adv. Mater.* **1999**, *11*, 579.
(49) Yun, H.-S.; Miyazawa, K.; Zhou, H.; Honma, I.; Kuwabara, M. *Adv. Mater.* **2001**, *13*, 1377.
(50) Zelcer, A.; Soler-Illia, G. J. A. A. *J. Mater. Chem. C* **2013**, *1*, 1359.
(51) Koh, C. W.; Lee, U. H.; Song, J. K.; Lee, H. R.; Kim, M. H.; Suh, M.; Kwon, Y. U. *Chem.–Asian. J.* **2008**, *3*, 862.
(52) Rathousky, J.; Kalousek, V.; Kolar, M.; Jirkovsky, J. *Photochem. Photobiol. Sci.* **2011**, *10*, 419.
(53) Grosso, D. *J. Mater. Chem.* **2011**, *21*, 17033.
(54) Fisher, A.; Kuemmel, M.; Järn, M.; Linden, M.; Boissière, C.; Nicole, L.; Sanchez, C.; Grosso, D. *Small* **2006**, *4*, 569.
(55) Soler-Illia, G. J. A. A.; Innocenzi, P. *Chem. Eur. J.* **2006**, *12*, 4478.
(56) Kuemmel, M.; Grosso, D.; Boissiere, C.; Smarsly, B.; Brezesinski, T.; Albouy, P. A.; Amenitsch, H.; Sanchez, C. *Angew. Chem., Int. Ed.* **2005**, *44*, 4589.
(57) Oveisi, H.; Jiang, X.; Imura, M.; Nemoto, Y.; Sakamoto, Y.; Yamauchi, Y. *Angew. Chem., Int. Ed.* **2011**, *50*, 7410.
(58) Jiang, X.; Suzuki, N.; Bastakoti, B. P.; Wu, K. C.-W.; Yamauchi, Y. *Chem.-Asian. J.* **2012**, *7*, 1713.
(59) Brezesinski, K.; Ostermann, R.; Hartmann, P.; Perlich, J.; Brezesinski, T. *Chem. Mater.* **2010**, *22*, 3079.
(60) Brezesinski, T.; Erpen, C.; Iimura, K. I.; Smarsly, B. *Chem. Mater.* **2005**, *17*, 1683.
(61) Brezesinski, T.; Antonietti, M.; Groenewolt, M.; Pinna, N.; Smarsly, B. *New J. Chem.* **2005**, *29*, 237.
(62) Brezesinski, T.; Wang, J.; Senter, R.; Brezesinski, K.; Dunn, B.; Tolbert, S. H. *ACS Nano* **2010**, *4*, 967.
(63) Müller, G.; Boissière, C.; Grosso, D.; Ringuedé, A.; Laberty-Robert, C.; Sanchez, C. *J. Mater. Chem.* **2012**, *22*, 9368.
(64) Haetge, J.; Reitz, C.; Suchomski, C.; Brezesinski, T. *RSC Adv.* **2012**, *2*, 7053.
(65) Castro, Y.; Julian, B.; Boissiere, C.; Viana, B.; Amenitsch, H.; Grosso, D.; Sanchez, C. *Nanotechnology* **2007**, *18*, 055705.
(66) Brezesinski, T.; Fattakhova-Rohlfing, D.; Sallard, S.; Antonietti, M.; Smarsly, B. M. *Small* **2006**, *2*, 1203.

(67) Chang, C.-Y.; Wang, C.-H.; Tseng, C.-J.; Cheng, K.-W.; Hourng, L.-W.; Tsai, B.-T. *International J. Hydrogen Energy* **2012**, *37*, 13616.

(68) Brezesinski, T.; Groenewolt, M.; Antonietti, M.; Smarsly, B. *Angew. Chem., Int. Ed.* **2006**, *45*, 781.

(69) Brezesinski, T.; Smarsly, B.; Iimura, K. I.; Grosso, D.; Boissière, C.; Amenitsch, H.; Antonietti, M.; Sanchez, C. *Small* **2005**, *1*, 889.

(70) Ortel, E.; Reier, T.; Strasser, P.; Kraehnert, R. *Chem. Mater.* **2011**, *23*, 3201.

(71) Haetge, J.; Hartmann, P.; Brezesinski, K.; Janek, J.; Brezesinski, T. *Chem. Mater.* **2011**, *23*, 4384.

(72) Eckhardt, B.; Ortel, E.; Polte, J.; Bernsmeier, D.; Gorke, O.; Strasser, P.; Kraehnert, R. *Adv. Mater.* **2012**, *24*, 3115.

(73) Brezesinski, T.; Wang, J.; Tolbert, S. H.; Dunn, B. *Nature Mater.* **2010**, *9*, 146.

(74) Yang, P. D.; Zhao, D. Y.; Margolese, D. I.; Chmelka, B. F.; Stucky, G. D. *Chem. Mater.* **1999**, *11*, 2813.

(75) Yang, P. D.; Zhao, D. Y.; Margolese, D. I.; Chmelka, B. F.; Stucky, G. D. *Nature* **1998**, *396*, 152.

(76) Brezesinski, K.; Wang, J.; Haetge, J.; Reitz, C.; Steinmueller, S. O.; Tolbert, S. H.; Smarsly, B. M.; Dunn, B.; Brezesinski, T. *J. Am. Chem. Soc.* **2010**, *132*, 6982.

(77) Lin, K. M.; Chang, K. H.; Hu, C. C.; Li, Y. Y. *Electrochim. Acta* **2009**, *54*, 4574.

(78) Shao, S.; Dimitrov, M.; Guan, N.; Köhn, R. *Nanoscale* **2010**, *2*, 2054.

(79) Brezesinski, T.; Fischer, A.; Iimura, K.-I.; Sanchez, C.; Grosso, D.; Antonietti, M.; Smarsly, B. M. *Adv. Funct. Mater.* **2006**, *16*, 1433.

(80) Jin, Z.; Zhou, H.-J.; Jin, Z.-L.; Savinell, R. F.; Liu, C.-C. *Sensors and Actuators B* **1998**, *52*, 188.

(81) Wang, Y.; Brezesinski, T.; Antonietti, M.; Smarsly, B. *ACS Nano* **2009**, *3*, 1373.

(82) Grosso, D.; Boissiere, C.; Smarsly, B.; Brezesinski, K.; Pinna, N.; Albouy, P. A.; Amenitsch, H.; Antonietti, M.; Sanchez, C. *Nat. Mater.* **2004**, *3*, 787.

(83) Sassoye, C.; Laberty, C.; Khanh, H. L.; Cassaignon, S.; Boissiere, C.; Antonietti, M.; Sanchez, C. *Adv. Funct. Mater.* **2009**, *19*, 1922.

(84) Crepaldi, E. L.; Soler-Illia, G. J. A. A.; Grosso, D.; Cagnol, F.; Ribot, F.; Sanchez, C. *J. Am. Chem. Soc.* **2003**, *125*, 9770.

(85) Grosso, D.; Soler-Illia, G. J. A. A.; Crepaldi, E. L.; Cagnol, F.; Sinturel, C.; Bourgeois, A.; Brunet-Bruneau, A.; Amenitsch, H.; Albouy, P. A.; Sanchez, C. *Chem. Mater.* **2003**, *15*, 4562.

(86) Zhang, J.; Deng, Y.; Gu, D.; Wang, S.; She, L.; Che, R.; Wang, Z.-S.; Tu, B.; Xie, S.; Zhao, D. *Adv. Energy Mater.* **2011**, *1*, 241.

(87) Smarsly, B.; Grosso, D.; Brezesinski, T.; Pinna, N.; Boissiere, C.; Antonietti, M.; Sanchez, C. *Chem. Mater.* **2004**, *16*, 2948.

(88) Wang, X. C.; Yu, J. C.; Hou, Y. D.; Fu, X. Z. *Adv. Mater.* **2005**, *17*, 99.

(89) Alberius, P. C. A.; Frindell, K. L.; Hayward, R. C.; Kramer, E. J.; Stucky, G. D.; Chmelka, B. F. *Chem. Mater.* **2002**, *14*, 3284.

(90) Crepaldi, E. L.; Soler-Illia, G. J. A. A.; Grosso, D.; Sanchez, C. *New J. Chem.* **2003**, *27*, 9.

(91) Angelomé, P. C.; Andrini, L.; Calvo, M. E.; Requejo, F. G.; Bilmes, S. A.; Soler-Illia, G. J. A. A. *J. Phys. Chem. C* **2007**, *111*, 10886−10893.

(92) Violi, I. L.; Perez, M. D.; Fuertes, M. C.; Soler-Illia, G. J. A. A. *ACS Appl. Mater. Interfaces* **2012**, *4*, 4320.

(93) Martinez-Ferrero, E.; Grosso, D.; Boissiere, C.; Sanchez, C.; Oms, O.; Leclercq, D.; Vioux, A.; Miomandre, F.; Audebert, P. *J. Mater. Chem.* **2006**, *16*, 3762.

(94) Ko, Y.-S.; Koh, C.-W.; Lee, U.-H.; Kwon, Y. U. *Microporous Mesoporous Mater.* **2011**, *145*, 141.

(95) Liu, D.; Lei, J.-H.; Guo, L.-P.; Deng, K.-J. *Microporous Mesoporous Mater.* **2001**, *139*, 87.

(96) Choi, S. Y.; Mamak, M.; Coombs, N.; Chopra, N.; Ozin, G. A. *Adv. Funct. Mater.* **2004**, *14*, 335.

(97) Choi, S. Y.; Lee, B.; Carew, D. B.; Mamak, M.; Peiris, F. C.; Speakman, S.; Chopra, N.; Ozin, G. A. *Adv. Funct. Mater.* **2006**, *16*, 1731.

(98) Wu, C. W.; Ohsuna, T.; Kuwabara, M.; Kuroda, K. *J. Am. Chem. Soc.* **2006**, *128*, 4544.

(99) Docampo, P.; Stefik, M.; Guldin, S.; Gunning, R.; Yufa, N. A.; Cai, N.; Wang, P.; Steiner, U.; Wiesner, U.; Snaith, H. J. *Adv. Energy Mater.* **2012**, *2*, 676.
(100) Soler-Illia, G. J. A. A.; Louis, A.; Sanchez, C. *Chem. Mater.* **2002**, *14*, 750.
(101) Luo, H.; Wang, C.; Yan, Y. *Chem. Mater.* **2003**, *15*, 3841.
(102) Leroy, C. M.; Cardinal, T.; Jubera, V.; Treguer-Delapierre, M.; Majimel, J.; Manaud, J. P.; Backov, R.; Boissiere, C.; Grosso, D.; Sanchez, C.; Viana, B.; Pellé, F. *Chem. Phys. Chem.* **2008**, *9*, 2077.
(103) Dros, A. B.; Grosso, D.; Boissiere, C.; Soler-Illia, G. J. A. A.; Albouy, P.-A.; Amenitsch, H.; Sanchez, C. *Microporous Mesoporous Mater.* **2006**, *94*, 208.
(104) Ortiz de Zarate, D.; Boissiere, C.; Grosso, D.; Albouy, P. A.; Amenitsch, H.; Amoros, P.; Sanchez, C. *New. J. Chem.* **2005**, *29*, 141.
(105) Puangpetch, T.; Chavadej, S.; Sreethawong, T. *Powder Technol.* **2011**, *208*, 37.
(106) Cheng, W.; Baudrin, E.; Dunn, B.; Zink, J. I. *J. Mater. Chem.* **2001**, *11*, 92.
(107) Ying, B.; Zhang, Y.; Drabarek, E.; Barnes, P. R. F.; Luca, V. *Chem. Mater.* **2007**, *19*, 5664.
(108) Sallard, S.; Brezesinski, T.; Smarsly, B. M. *J. Phys. Chem. C* **2007**, *111*, 7200.
(109) Cui, X.; Hua, Z.; Wei, C.; Shu, Z.; Zhang, L.; Chen, H.; Shi, J. *Chem. Asian J.* **2013**, *8*, 429.
(110) Deepa, M.; Srivastava, A. K.; Agnihotry, S. A. *Acta Materialia* **2006**, *54*, 4583.
(111) Yuan, Q.; Li, L.-L.; Lu, S.-L.; Duan, H.-H.; Li, Z.-X.; Zhu, Y.-X.; Yan, C.-H. *J. Phys. Chem. B* **2009**, *113*, 4117.
(112) Castro, Y.; Juliàn-Lopez, B.; Boissiere, C.; Viana, B.; Grosso, D.; Sanchez, C. *Microporous Mesoporous Mater.* **2007**, *103*, 273.
(113) Miko, A.; Demirel, A. L.; Somer, M. *J. Mater. Chem.* **2012**, *22*, 3705.
(114) Leroy, C. M.; Cardinal, T.; Jubera, V.; Aymonier, C.; Treguer-Delapierre, M.; Boissiere, C.; Grosso, D.; Sanchez, C.; Viana, B.; Pellé, F. *Microporous Mesoporous Mater.* **2013**, *170*, 123.
(115) Li, D.; Zhou, H.; Honma, I. *Nat. Mater.* **2004**, *3*, 65.
(116) Kirsch, B. L.; Richman, E. K.; Riley, A. E.; Tolbert, S. H. *J. Phys. Chem. B* **2004**, *108*, 12698.
(117) Dong, W.; Sun, Y.; Lee, C. W.; Hua, W.; Lu, X.; Shi, Y.; Zhang, S.; Chen, J.; Zhao, D. *J. Am. Chem. Soc.* **2007**, *129*, 13894.
(118) Miyata, H.; Fukushima, Y.; Okamoto, K.; Takahashi, M.; Watanabe, M.; Kubo, W.; Komoto, A.; Kitamura, S.; Kanno, Y.; Kuroda, K. *J. Am. Chem. Soc.* **2011**, *133*, 13539.
(119) Fattakhova-Rohlfing, D.; Wark, M.; Brezesinski, T.; Smarsly, B. M.; Rathouský, J. *Adv. Funct. Mater.* **2007**, *17*, 123.
(120) Uchida, H.; Patel, M. N.; May, R. A.; Gupta, G.; Stevenson, K. J.; Johnston, K. P. *Thin Solid Films* **2010**, *518*, 3169.
(121) Agarwala, S.; Kevin, M.; Wong, A. S. W.; Peh, C. K. N.; Thavasi, V.; Ho, G. W. *ACS Appl. Mater. Interfaces* **2010**, *2*, 1844.
(122) Kajihara, K.; Yao, T. J. *Sol-Gel Sci. Technol.* **2000**, *17*, 173.
(123) Wang, K. *Chem. Mater.* **2005**, *17*, 4825.
(124) Boissière, C.; Grosso, D.; Lepoutre, S.; Nicole, L.; Bruneau, A. B.; Sanchez, C. *Langmuir* **2005**, *21*, 12362.
(125) Huo, Q.; Margolese, D. I.; Ciesla, U.; Demuth, D. G.; Feng, P.; Gier, T. E.; Sieger, P.; Firouzi, A.; Chmelka, B. F.; Schüth, F.; Stucky, G. D. *Chem. Mater.* **1994**, *6*, 1176.
(126) Kuemmel, M.; Smatt, J. H.; Boissiere, C.; Nicole, L.; Sanchez, C.; Linden, M.; Grosso, D. *J. Mater. Chem.* **2009**, *19*, 3638.
(127) Luca, V.; Drabarek, E.; Griffith, C. S.; Hanley, T. L. *Chem. Mater.* **2010**, *22*, 3832.
(128) Faustini, M.; Louis, B.; Albouy, P. A.; Kuemmel, M.; Grosso, D. *J. Phys. Chem C* **2010**, *114*, 7637.
(129) Wiebcke, M.; Grube, M.; Koller, H.; Engelhardt, G.; Felsche, J. *Microporous Mater.* **1993**, *2*, 55.
(130) Bass, J. D.; Grosso, D.; Boissiere, C.; Sanchez, C. *J. Am. Chem. Soc.* **2008**, *130*, 7882.
(131) Müller, V.; Rasp, M.; Rathouský, J.; Schütz, B.; Niederberger, M.; Fattakhova-Rohlfing, D. *Small* **2010**, *6*, 633.

(132) Brezesinski, T.; Wang, J.; Polleux, J.; Dunn, B.; Tolbert, S. H. *J. Am. Chem. Soc.* **2009**, *131*, 1802.
(133) Corma, A.; Atienzar, P.; Garcia, H.; Chane-Ching, J.-Y. *Nat. Mater.* **2004**, *3*, 394.
(134) Deshpande, A. S.; Pinna, N.; Smarsly, B.; Antonietti, M.; Niederberger, M. *Small* **2005**, *1*, 313.
(135) Hosseingholi, M.; Pazouki, M.; Hosseinnia, A.; Aboutalebi, S. H. *J. Phys. D: Appl. Phys.* **2011**, *44*, 055402.
(136) Bleta, R.; Alphonse, P.; Lorenzato, L. *J. Phys. Chem. C* **2010**, *114*, 2039.
(137) Bosc, F.; Ayral, A.; Albouy, P. A.; Guizard, C. *Chem. Mater.* **2003**, *15*, 2463.
(138) Deshpande, A. S.; Pinna, N.; Beato, P.; Antonietti, M.; Niederberger, M. *Chem. Mater.* **2004**, *16*, 2599.
(139) Hartmann, P.; Lee, D.-K.; Smarsly, B. M.; Janek, J. *ACS Nano* **2010**, *4*, 3147.
(140) Aksay, I. A.; Trau, M.; Manne, S.; Honma, I.; Yao, N.; Zhou, L.; Fenter, P.; Eisenberger, P. M.; Gruner, S. M. *Science* **1996**, *273*, 892.
(141) Kawashima, Y.; Nakagawa, M.; Ichimura, K.; Seki, T. *J. Mater. Chem.* **2004**, *14*, 328.
(142) Hillhouse, H. W.; Okubo, T.; van Egmond, J. W.; Tsapatsis, M. *Chem. Mater.* **1997**, *9*, 1505.
(143) Koganti, V. R.; Rankin, S. E. *J. Phys. Chem. B* **2005**, *109*, 3279.
(144) Freer, E. M.; Krupp, L. E.; Hinsberg, W. D.; Rice, P. M.; Hedrick, J. L.; Cha, J. N.; Miller, R. D.; Kim, H. C. *Nano Lett.* **2005**, *5*, 2014.
(145) Brinker, C. J.; Dunphy, D. R. *Current Opinion Colloid Interface Sci.* **2006**, *11*, 126.
(146) Miyata, H.; Kobori, S.; Kubo, W.; Watanabe, M.; Kuroda, K. *Langmuir* **2013**, *29*, 761.
(147) Wu, K. C.-W.; Jiang, X.; Yamauchi, Y. *J. Mater. Chem.* **2011**, *21*, 8934.
(148) Jiang, X.; Ishizumi, A.; Suzuki, N.; Naito, M.; Yamauchi, Y. *Chem. Commun.* **2012**, *48*, 549.
(149) Richman, E. K.; Brezesinski, T.; Tolbert, S. H. *Nature Mater.* **2008**, *7*, 712.
(150) Yamauchi, Y.; Nagaura, T.; Ishikawa, A.; Chikyow, T.; Inoue, S. *J. Am. Chem. Soc.* **2008**, *130*, 10165.
(151) Yamauchi, Y.; Nagaura, T.; Inoue, S. *Chem. Asian J.* **2009**, *4*, 1059.
(152) Hara, M.; Nagano, S.; Seki, T. *J. Am. Chem. Soc.* **2010**, *132*, 13654.
(153) Brezesinski, T.; Groenewolt, M.; Pinna, N.; Amenitsch, H.; Antonietti, M.; Smarsly, B. M. *Adv. Mater.* **2006**, *18*, 1827.
(154) Zhang, Y.; Li, J.; Wang, J. *Chem. Mater.* **2006**, *18*, 2917−2923.
(155) Pärna, R.; Joost, U.; Nõmmiste, E.; Käämbre, T.; Kikas, A.; Kuusik, I.; Kink, I.; Hirsimäki, M.; Kisand, V. *Phys. Status Solidi A* **2012**, *209*, 953.
(156) Chen, F.; Deng, H. M.; Huang, D. J.; Yang, P. X.; Chu, J. H. *J. Phys.: Conf. Ser.* **2011**, *276*, 012160.
(157) Bassiri-Gharb, N.; Bastani, Y.; Bernal, A. *Chem. Soc. Rev.* **2014**, *43*, 2125.
(158) Dawber, M.; Rabe, K. M.; Scott, J. F. *Rev. Mod. Phys.* **2005**, *77*, 1083.
(159) Vrejoiu, I.; Alexe, M.; Hesse, D.; Gösele, U. *Adv. Funct. Mater.* **2008**, *18*, 3892.
(160) Moreno, C.; Abellàn, P.; Hassini, A.; Ruyter, A.; Pérez del Pino, A.; Sandiumenge, F.; Casanove, M.-J.; Santiso, J.; Puig, T.; Obradors, X. *Adv. Funct. Mater.* **2009**, *19*, 2139.
(161) Carretero-Genevrier, A.; Gàzquez, J.; Puig, T.; Mestres, N.; Sandiumenge, F.; Obradors, X.; Ferain, E. *Adv. Funct. Mater.* **2010**, *20*, 892.
(162) Brinker, C. J.; Clem, P. G. *Science* **2013**, *340*, 818.
(163) Tadigadapa, S.; Mateti, K. *Meas. Sci. Technol.* **2009**, *20*, 092001.
(164) Matusita, K.; Tashiro, M. *J. Non-Crystalline Solids* **1973**, *11*, 471.
(165) Phalippou, J.; Prassas, M.; Zarzycki, J. *J. Non-Crystalline Solids* **1982**, *48*, 17.
(166) Congshan, Z.; Phalippou, J.; Zarzycki, J. *J. Non-Crystalline Solids* **1986**, *82*, 321.
(167) Drisko, G. L.; Carretero-Genevrier, A.; Perrot, A.; Gich, M.; Gàzquez, J.; Rodriguez-Carvajal, J.; Favre, L.; Grosso, D.; Boissiere, C.; Sanchez, C. **submitted**.
(168) Bertone, J. F.; Cizeron, J.; Wahi, R. K.; Bosworth, J. K.; Colvin, V. L. *Nano Lett.* **2003**, *3*, 655.
(169) Mohamed, K.; Alkaisi, M. M. *Nanotechnology* **2013**, *24*, 015302.
(170) Minnick, M. D.; Devenyi, G. A.; Kleiman, R. N. *J. Micromech. Microeng.* **2013**, *23*, 117002.
(171) Anderson, O. L.; Stuart, D. A. *J. Am. Ceramic Soc.* **1954**, *37*, 573.

(172) Carretero-Genevrier, A.; Oro-Sole, J.; Gàzquez, J.; Magén, C.; Miranda, L.; Puig, T.; Obradors, X.; Ferain, E.; Sanchez, C.; Rodriguez-Carvajal, J.; Mestres, N. *Chem. Mater.* **2014**, *26*, 1019.
(173) Carretero-Genevrier, A.; Mestres, N.; Puig, T.; Hassini, A.; Oro, J.; Pomar, A.; Sandiumenge, F.; Obradors, X.; Ferain, E. *Adv. Mater.* **2008**, *20*, 3672.
(174) Carretero-Genevrier, A.; Gàzquez, J.; Idrobo, J. C.; Oro, J.; Arbiol, J.; Varela, M.; Ferain, E.; Rodriguez-Carvajal, J.; Puig, T.; Mestres, N.; Obradors, X. *J. Am. Chem. Soc.* **2011**, *133*, 4053.
(175) Carretero-Genevrier, A.; Puig, T.; Obradors, X.; Mestres, N. *Chem. Soc. Rev.* **2014**, *43*, 2042.
(176) Inagaki, S.; Guan, S.; Ohsuna, T.; Terasaki, O. *Nature* **2002**, *416*, 304.

Biographies :

Dr Cédric Boissière obtained his PhD in developing sol-gel for separations at the European Institute of Membranes in Montpellier. Since 2002 he has worked in the Laboratory of Chimie de la Matière Condensée de Paris on the synthesis of functional hierarchical nano-materials by coupling evaporation processing and bottom-up soft-chemistry. Most of his achievements concern nanostructured thin films, nanoparticles and aerosol materials for optics, heterogeneous catalysis and nanomedicine. He is co-author of 140 articles and 25 patents. His work was recognized by the European Membrane Society in 2006, the Jean RIST medal of the SF2M in 2007, and the Award of French Chemistry Society in 2014.

Dr Glenna L. Drisko obtained her PhD in 2010 from The University of Melbourne where she studied morphological control of sol-gel derived materials using organic templates. She spent 3 years as a post-doctorate researcher in the LCMCP studying the synthesis and optical properties of structured thin films and the crystallization of mesostructured silica. Since the beginning of 2014 she has been working on the synthesis of metal and metal oxide nanoparticles in organic media in the Laboratoire de Chimie de Coordination. She has won the Albert Shimmins Award (2009), ARNAM's Best Oral Presentation (2008) and Best Rabbit Showmanship at the Humboldt County Fair (1998).

David Grosso was appointed full-professor in 2007 at the University of Paris. He leads the team working at the interface between Chemistry and Processing at the Laboratoire Chimie de la Matière Condensée de Paris (UPMC-Collège de France). Most of his achievements concern nanostructured thin films and aerosol materials prepared through liquid processing approaches. His work was awarded by the International Sol-gel Society in 2005 and by the French Society of Chemistry in 2009. He is a junior member of the French Institute of University since 2009, and he is co-founder of two start-up companies.

Adrián Carretero Genevrier is a permanent CNRS researcher at the Institute of Nanotechnology in Lyon (INL). He obtained his PhD in 2010 in materials science from the Universitat Autònoma de Barcelona and then spent three postdoctoral years at the Collège de France. His research is aimed at understanding the growth mechanisms of new complex oxide nanostructures synthesized by soft chemistry and the relationship between crystal structure and physical properties. His scientific interests include soft chemistry routes to grow functional oxide nanomaterials, crystal engineering, nanofabrication, template-assisted synthesis of inorganic gels, mesoporous coating, crystalline nanostructured oxide coatings and mesoporous materials for catalysis.

Prof. Clément Sanchez at the Collège de France is the Chair of the Chemistry of Hybrid Materials. He was previously the director of the LCMCP, director of research at the French Research Council, and professor at l'Ecole Polytechnique. At the Collège de France he specializes in nanochemistry, the physical properties of nanostructured porous and non-porous transition metal oxide based gels, and porous and non-porous hybrid organic inorganic materials shaped as monoliths, microspheres and films. He was the recipient of many national and international awards and is a member of French, European, and Spanish Academies of Science.